Proceedings of the 5th International Conference on Nanotechnology: Fundamentals and Applications
Prague, Czech Republic, August 11-13, 2014
Paper No. 265

On the Accuracy of Residual Stress Evaluation from Focused Ion Beam DIC (FIB-DIC) Ring-core Milling Experiments

Enrico Salvati, Tan Sui, Siqi Ying, Alexander J.G. Lunt, Alexander M. Korsunsky
Department of Engineering Science, University of Oxford
Parks Road, Oxford OX1 3PJ, UK
enrico.salvati@eng.ox.ac.uk; tan.sui@eng.ox.ac.uk; siqi.ying@eng.ox.ac.uk;
alexander.lunt@eng.ox.ac.uk; alexander.korsunsky@eng.ox.ac.uk

Abstract – Focused Ion Beam (FIB) milling offers a means of material removal at the nanoscale with minimal disturbance. This opens up a family of residual stress evaluation techniques that rely on the combination of strain relief measurement and deformation modelling. A particular flavour of the nanoscale strain relief methodology is offered by the ring-core milling proposed by Korsunsky et al (2009). In this study we present the results of finite element modelling (FEM) of the strain redistribution at the surface of the central circular "island" produced by FIB milling of the annular trench around it. The results demonstrate that the strain distribution at the "island" surface that is homogeneous before milling goes through an evolution that makes it non-uniform, with the greatest relief occurring at the periphery. However, as the trench depth approaches the value of the island diameter, the strain distribution becomes uniform again, and approaches fully relieved state ("zero strain"). The regions of the surface that lie close to the "island" periphery are the most prone to FIB damage and may not be suitable for DIC interpretation. A new depth profile curve was calculated based on the DIC analysis confined to 80% of the radial extent. The curve differs significantly from that previously reported for the full 100% use of the "island" area, notably by virtue of showing parabolic behaviour as a function of normalised depth at early stages of milling. The implications of this result for the inverse problem analysis (residual stress depth profiling) are discussed.

***Keywords*:** FIB, FEM, Residual stress.

1. Introduction

Residual stresses play a crucial role in determining the deformation behaviour and performance of engineering components and materials, from bulk alloys and composites used in construction and manufacturing industries down to the stresses within individual grains of polycrystalline aggregates. During service, the associated residual stresses may combine with applied stresses to cause damage initiation and failure, or to shorten the component lifetime. Residual stresses exist across the scales, from macroscopic to nanometre. All kinds of residual stresses are caused by the presence of incompatible strains within the material. Analytically the incompatibility is best described via internal misfit strains, usually called eigenstrains (Mura, 1987). Eigenstrain can be induced by many inelastic processes such as plastic deformation, thermal expansion mismatch, or crystallographic transformations that occur within different parts of components during manufacturing and processing. These may result from material cutting and pasting operations (cf. welding), or arise as a consequence of the local anisotropy or inhomogeneity of stiffness, yield stress or thermal expansion coefficient. Knowing how the eigenstrain is distributed within the material is vital to understanding the residual stresses. Eigenstrain modelling is a powerful analytical technique for the representation of residual stress states in solids. A practical approach to the use of eigenstrain in residual stress modelling can be developed based on the basic postulates presented by Korsunsky (2009). Due to the simplicity of the physical mechanism and the mathematical description of thermal expansion mismatch, thermal strains are usually chosen to represent eigenstrain in order to study the corresponding residual stress distributions. Thermal strain is expressed as:

$$\vec{\varepsilon}_{\text{thermal}} = \vec{\alpha}(T_{\text{final}} - T_{initial}) \quad (1)$$

where $\bar{\alpha}$ is the tensor of the coefficients of linear thermal expansion, which contains **six** independent parameters. Therefore, by introducing a spatially varying field $\bar{\alpha}$ and applying a uniform temperature change, arbitrary eigenstrain field can be readily implemented within a FEM. The residual stress in any region can then be calculated by the thermo-elastic (NB: not incremental) FEM calculation. Following strain measurement after material removal (i.e. FIB-milling procedure), the incremental milling process can be simulated by progressive element deactivation around the region. Note that whilst residual stress is altered in response to the change of boundary conditions, the underlying eigenstrain field remains unchanged, provided the material removal process does not lead to the introduction of additional misfit strain (eigenstrain). We note that for the case of relatively large FIB-milled features this is a valid approximation. For example, whilst the depth of Ga-ion implantation in most materials is expected not to exceed 100nm, typical milled features are at least one or two orders of magnitude larger, in the micron range. In the discussion presented below it is assumed explicitly that no introduction of additional eigenstrain, nor any modification of the prior existing eigenstrain occurs during FIB milling.

2. Modelling

A 3-D ring-core milling model was created to simulate the residual stress state evolution during incremental milling by finite element (FE) simulation using commercial package ABAQUS® 6.12. The incremental milling process was simulated by setting the material properties of the milled region to be equal to those of air. The ring-core drilling model was established in a 100μm×100μm×100μm cubic material volume. In order to reduce the computational effort, taking advantage of the symmetry condition, only a quarter of the volume was modelled. A cylindrical region in the middle was partitioned as follows. A "stack" of annular domains with the inner radius of 20 μm and outer radius of 30 μm was prepared, as illustrated in Fig. 1. The annular domain corresponds to the volume to be removed by milling. Fig. 1 illustrates each annular layer with the thickness of 1 μm removed at each step. The total maximum milling depth was set to 20 μm, i.e. 20-step ring core-milling was simulated as shown in Fig. 1. The surface of the inner core region ("island") in Fig. 1 represents the area for which the strain evolution is being monitored during incremental milling. In Fig. 1, the 16 μm diameter circle is also shown for the purpose of strain calculation over the 80% radial extent, as described further below.

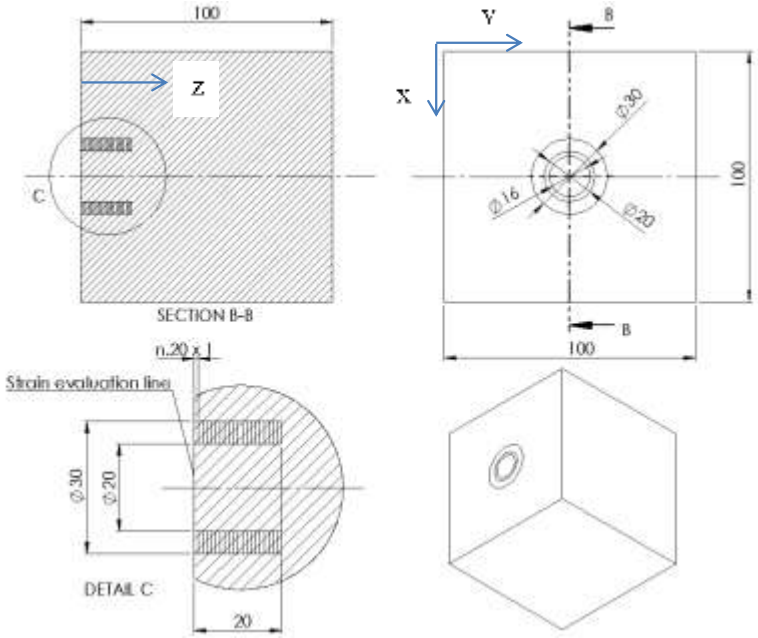

Fig. 1.Illustration of the 3-D ring-core drilling CAE model.

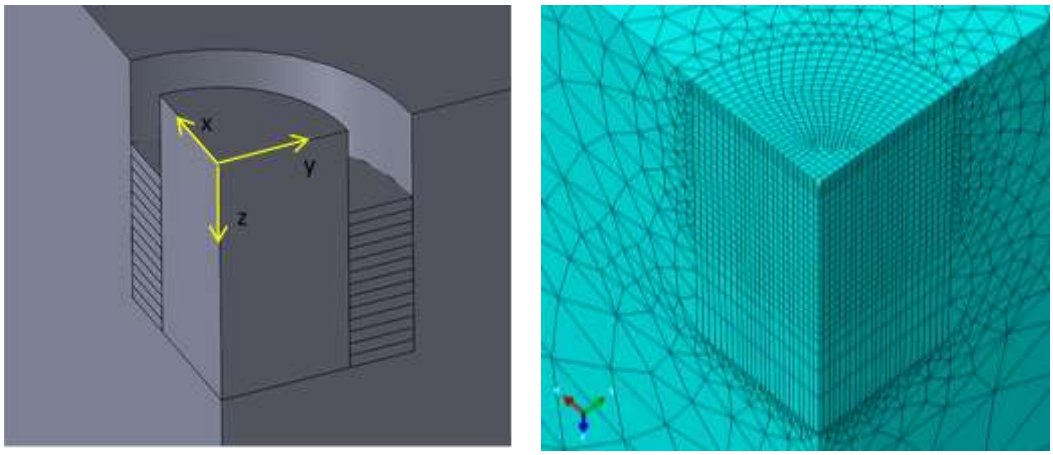

(a) (b)

Fig. 2: Illustration of the 3-D ring-core drilling FEM model. (a) Progressive removal of milled layer at each step. (b) Illustration of the FE mesh in the zone of interest.

The bulk material was assumed to have the properties of stainless steel with an elastically anisotropic fcc structure. The stiffness matrix (*C*) of the material is given below (2) in the units of MPa (Li and Dowd, 2011). For simplicity, initially the local "crystal" coordinate (shown in yellow in Fig. 2.a) was aligned with the global coordinate (shown in RGB coding in Fig. 2b). Thus, the orientation of global coordinate axes with respect to the material crystal axes were assumed to correspond to the directions with Miller indices (100), (010) and (001). Other orientations can be readily defined by applying a rotation matrix *T* that describes the transformation from global to local coordinates to the original stiffness matrix (*C*). The material properties of the empty space (where material was removed by milling) were set to isotropic with Young's modulus E_{air}=0.001 MPa and Poisson's ratio ν_{air} =0.001.

$$C = \begin{bmatrix} 198000 & 125000 & 125000 & 0 & 0 & 0 \\ 125000 & 198000 & 125000 & 0 & 0 & 0 \\ 125000 & 125000 & 198000 & 0 & 0 & 0 \\ 0 & 0 & 0 & 122000 & 0 & 0 \\ 0 & 0 & 0 & 0 & 122000 & 0 \\ 0 & 0 & 0 & 0 & 0 & 122000 \end{bmatrix} \quad (2)$$

Anisotropic coefficients of thermal expansion (CTE) were used in the simulation as follows:

$$\vec{\alpha} = [\alpha_1, \alpha_2, \alpha_3, \alpha_4, \alpha_5, \alpha_6] \quad (3)$$

where $\alpha_1, \alpha_2, \alpha_3$ represent the linear thermal expansion coefficients along the *x*-, *y*- and *z*- axis respectively. In the simulation of expansion eigenstrain, $\alpha_1 = 0.025, \alpha_2 = 0.025, \alpha_3 = 0$ were assigned, while $\alpha_1 = -0.025, \alpha_2 = -0.025, \alpha_3 = 0$ were used to simulate the thermal contraction. The thermal expansion coefficients were considered to be uniform as a function of the *z* coordinate. However, since $\vec{\alpha}$ is assigned at the level of integration points (IP's), arbitrary spatial variation with depth *z* can be imposed.

3. Results

The bulk was assigned the above CTE, which allows the generation of pseudo-thermal strain to represent misfit or eigenstrain after imposing a uniform predefined temperature change. The evolution of the elastic strain values at the core surface (in-plane strains ε_{11} and ε_{22}) were calculated during

incremental milling. The results for both cases of contraction and expansion eigenstrain are presented in Fig. 3. For comparison in each case the average strain was computed over the entire central core island (referred to as 100%), and also in a smaller region with the diameter of 16 μm shown in Fig. 1, marked 80%. Choosing 80% of the diameter is a practical approximation of the conditions expected in FIB-DIC experiments, due to the likely beam damage at the edge of the core surface. In Fig. 4, the elastic strain evolution along the *z*-axis (ε_{33}, out-of-plane strain relief) is plotted.

The average results for the strain components along the *x*-axis and *y*-axis are almost identical. Similar consistency is also observed for the results of 100% and 80% core radius conditions. The results show an initial stage of approximately linear relaxation followed by a peak and subsequent gradual saturation. The strain value along *z*-axis is much smaller than those along *x*-axis and *y*-axis. The saturation strain is referred to as zero, indicating complete stain relief.

The fitting master function has been proposed that provides an analytical description of the relationship between the relief strain and the milling depth, i.e. the continuous strain relief curve illustrated in Fig. 3. It is given by:

$$f(\Delta\varepsilon_\infty, z) = \Delta\varepsilon_\infty \left[5.5\frac{z^2}{(1+z)^3}\left[1+\frac{2}{(1+z^4)}\right]-1\right] \quad (4)$$

The function is expressed in terms of the normalized depth parameter $z=(h/0.6d)$, where h is the drilling depth and d is the outer diameter of the remaining core "stub". The complete relief strain $\Delta\varepsilon_\infty$ is contained in the master function as a scaling parameter. Effectively, this simple analytical expression encapsulates the results of FE simulations. Generally, Eq. (4) can be used when a linear trend at the beginning of milling is observed. However, the actual initial non-linear phenomenon of the curves for the 80% core region observed in Fig. 3 for both contraction and expansion indicates that master function needs to be modified if e.g. 80% core radius is used for analysis.

Radial plots of the strain value along *x*-axis at different milling steps are shown in Fig. 5. It is observed that the radial variation of the strain is almost uniform at the first and last milling step, which is before milling and after the full milling respectively.

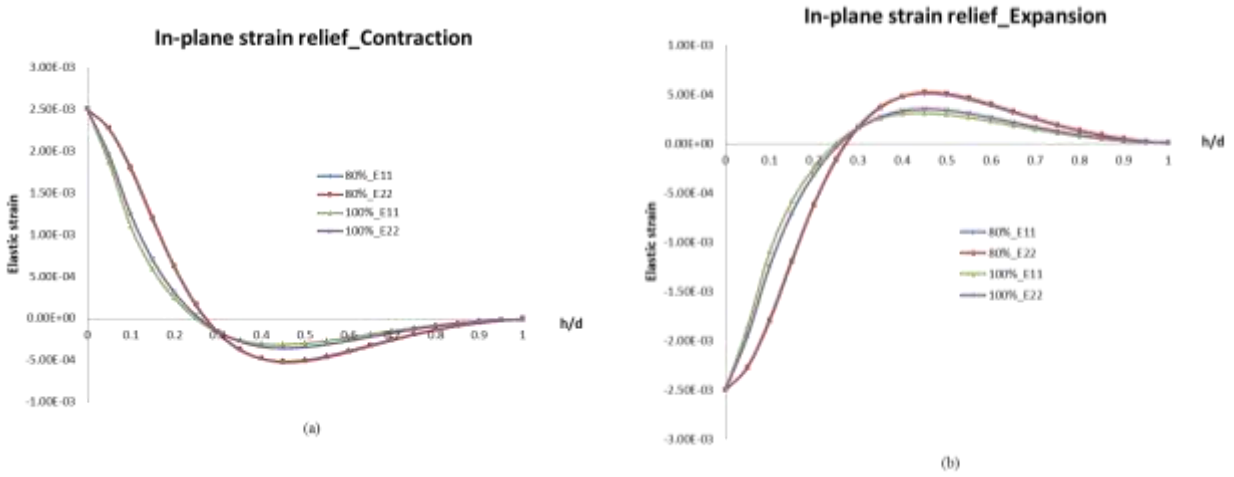

Fig. 3. Average elastic strain evolution: (a) contraction and (b) expansion for 80% and 100% radial extent.

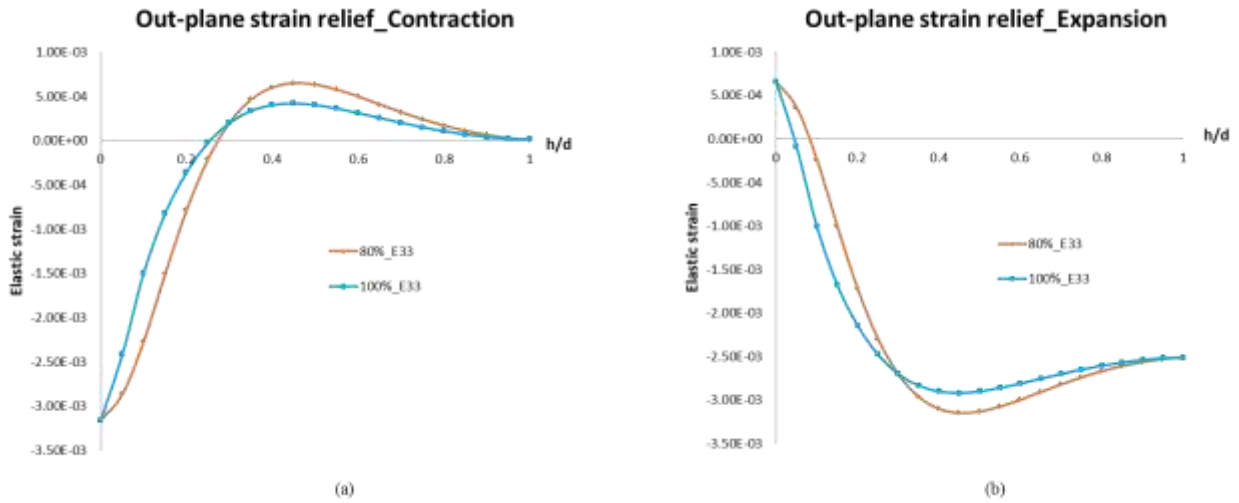

Fig. 4. Average elastic strain evolution: (a) contraction and (b) expansion for 80% and 100% of radial extent.

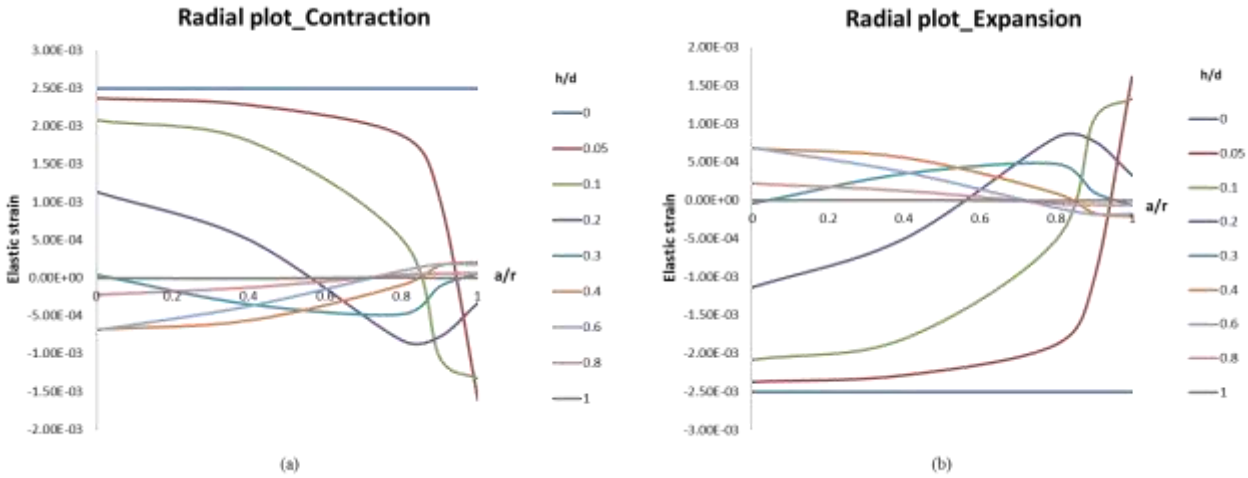

Fig. 5. Radial plot of strain distribution in the core surface at milling steps (a) contraction and (b) expansion.

4. Conclusion

Residual stress measurement was considered in this work by means of 3-D FEM analysis. A uniform 3-D residual stress field was imposed to the material through the eigenstrain method. The FEM results have shown that the greater relief of elastic strain at the surface occurs at the periphery of the ‘’island’’ (see Fig. 5). Such phenomenon gradually vanishes as milling depth approaches the diameter of the island.

During FIB milling, the external region of the ‘’island’’ is often damaged. For this reason, the average strain in a reduced area (80% of radius) is also calculated. Fig. 3 shows the difference profile shape between the 100% and the 80% area. Note that there is no difference in the full residual strain relief range, i.e. the starting and ending elastic strain values are consistent.

An improved new fitting function has been proposed for the strain profile, which can be used for the correlation of experimental results given by the DIC analysis.

One important conclusion to be drawn on from the results is that careful consideration must be given to the matter of choosing surface area for DIC strain evaluation before attempting the interpretation of residual stress profile in terms of residual stress depth variation.

References

Korsunsky A.M., Sebastiani M., Benporad E. (2009). Focused ion beam ring drilling for residual stress evaluation. Material Letters 63, 1961-1963,

Mura T. Micromechanics of Defects in Solids, Springer, 1987.

Korsunsky A.M. (2009), Eigenstrain analysis of residual strains and stresses, The Journal of Strain Analysis for Engineering Design. 01/2009; 44(1):29-43. DOI:10.1243/03093247JSA423

Li D.F., Dowd N.P.O. (2011) On the evolution of lattice deformation in austenitic stainless steels—The role of work hardening at finite strains, J Mech Phys Solids, 592421-2441.